Two-photon absorption and spectroscopy of the lowest two-photon transition in small donor-acceptor–substituted organic molecules

Marten T. Beels and Ivan Biaggio
Physics Department, Lehigh University, Bethlehem, Pennsylvania 18015, USA

Tristan Reekie, Melanie Chiu, and François Diederich
Laboratory of Organic Chemistry, Department of Chemistry and Applied Biosciences, ETH-Zürich, CH-8093 Zürich, Switzerland
(Received 31 December 2014; published 10 April 2015)

We determine the dispersion of the third-order polarizability of small donor-acceptor substituted organic molecules using wavelength-dependent degenerate four-wave mixing experiments in solutions with varying concentrations. We find that donor-acceptor–substituted molecules that are characterized by extremely efficient off-resonant nonlinearities also have a correspondingly high two-photon absorption cross section. The width and shape of the first two-photon resonance for these noncentrosymmetric molecules follows what is expected from their longest wavelength absorption peak, and the observed two-photon absorption cross sections are record high when compared to the available literature data, the size of the molecule, and the fundamental limit for two-photon absorption to the lowest excited state, which is essentially determined by the number of conjugated electrons and the excited-state energies. The two-photon absorption of the smallest molecule, which only has 16 electrons in its conjugated system, is one order of magnitude larger than for the molecule called AF-50, a reference molecule for two-photon absorption [O.-K. Kim *et al.*, Chem. Mater. **12**, 284 (2000)].

DOI: 10.1103/PhysRevA.91.043818 PACS number(s): 42.65.Hw, 78.47.nj, 71.20.Rv, 42.70.Jk

I. INTRODUCTION

The wavelength dependence of the complex third-order nonlinear optical polarizability (second hyperpolarizability) of a molecule contains information on the mechanisms of resonance enhancement of the optical nonlinearity and allows comparison of the peak two-photon absorption cross sections to the off-resonant third-order polarizabilities. In this work, we determine the dispersion of the third-order polarizabilities in donor-acceptor–substituted small organic molecules that have shown high off-resonant third-order nonlinearities both relative to the fundamental limit and relative to their molecular mass.

Third-order nonlinear optical effects basically mediate the interaction between four photons, as an example in a process where three photons interact to generate a fourth one. These effects are responsible for phenomena such as self-phase modulation, all-optical switching, or in general four-wave mixing [1–3]. Organic molecules are attractive as materials for nonlinear optics because their π-electron conjugation leads to very large third-order nonlinearities. These large nonlinearities can be off-resonant and essentially instantaneous compared to the period of an optical wave, or they can be observed for photon energies near half the optical excitation energy, when they deliver large two-photon absorption cross sections.

For a complete characterization of a nonlinear optical molecule it is important to determine its nonlinear response in the zero-frequency limit—the off-resonant case when the energy of the interacting photons is much smaller than the first optical excitation energy in a molecule—and then to study how the response changes as the photon energy increases towards the first optical resonance. The third-order polarizability used to describe the nonlinear response of a molecule, which is in general a complex tensor, is real-valued in the zero-frequency limit and acquires an imaginary part when moving away from the zero-frequency limit. Thus, a complete spectroscopy of the nonlinear optical response requires the determination of both the real and the imaginary part of the third-order polarizability. For the effects described in this work, the real part describes self- and cross-phase modulation, while the imaginary part is related to two-photon absorption.

Full spectroscopy of the complex third-order polarizability of a molecule is potentially a cumbersome investigation involving several independent measurements with laser pulses of many different wavelengths. In this work, we describe a semiautomatic procedure that allows the efficient determination of the nonlinear optical spectrum. This procedure is based on the continuous acquisition of a degenerate four-wave mixing (DFWM) signal while automatically scanning the wavelength of a tunable laser. We will show that all the data necessary to obtain the nonlinear optical spectrum can be collected in two automated wavelength scans while allowing the optical energy of the interacting pulses to fluctuate while tuning their wavelength. The data are then analyzed to obtain the final spectrum. Such a time-saving automatic procedure is important in order to allow the rapid characterization of new compounds.

In the next section we first describe the definitions and nomenclature we will use throughout this work. This is followed by a review of the compounds that we will investigate: three molecules that have previously shown exceptionally high third-order nonlinear optical properties in the off-resonant (zero-frequency) limit. Then, in Sec. IV we derive a fundamental limit for the lowest energy two-photon absorption cross section (peak imaginary part of the third-order polarizability) that will serve as a benchmark to evaluate the efficiency of each molecule. Next, we devote Secs. V and VI to the development of the experimental methods: we review DFWM in the presence of linear and two-photon absorption, describe the data acquisition system, and discuss the numerical method used to extract the wavelength dependent real and imaginary parts of the third-order polarizability from the data

acquired at different wavelengths and molecular concentrations. Finally, we present and discuss the experimental results for the dispersion of the complex third-order polarizabilities, in particular the experimental two-photon cross sections, which we will compare to the fundamental limit and the size of the molecules.

II. DEFINITIONS AND CONVENTIONS

The third-order polarization induced in matter by the optical electric field is written as

$$P_i^{(3)} = \epsilon_0 \sum_{ijkl=1}^{3} \chi_{ijkl}^{(3)} E_j E_k E_l, \tag{1}$$

where ϵ_0 is the electric constant, $\chi_{ijkl}^{(3)}$ is the third-order nonlinear optical susceptibility, and the E_i are the components of the optical electric field vector along the three Cartesian axes. In this work we use *Système International* (S.I.) units throughout and follow the conventions described in Refs. [2] and [3]. Third-order nonlinear optical effects are described in bulk materials by a frequency-dependent third-order susceptibility $\chi_{ijkl}^{(3)}(-\omega_4,-\omega_3,\omega_2,\omega_1)$ that relates the amplitude of a third-order nonlinear optical polarization at frequency ω_4 and wave vector $\mathbf{k}_4$ to the amplitudes of three interacting optical electric-field components at frequencies and wave vectors ω_i and $\mathbf{k}_i$ [1]. Examples of such nonlinear optical effects include third-harmonic generation, self-action phenomena like self-focusing and nonlinear absorption (optical limiting), information transfer from one optical wave to another (all-optical switching), and four-wave mixing [1–3].

The magnitude of the third-order susceptibility $\chi_{ijkl}^{(3)}(-\omega,-\omega,\omega,\omega)$ of a material consisting of a number density N of nonlinear optical molecules is

$$\chi_{ijkl}^{(3)}(N) = f^4 N \gamma_{ijkl}, \tag{2}$$

where f is a local field factor ($f = [n^2+2]/3$ in the Lorentz approximation, with n the refractive index of the material) and γ_{ijkl} is the third-order polarizability tensor of a molecule in the same coordinate system as $\chi_{ijkl}^{(3)}$. For randomly oriented molecules in solution the contribution of the molecular third-order polarizability to a diagonal element $\chi_{1111}^{(3)}$ is given by the scalar orientational average, $\gamma_{\rm rot}$, of the corresponding molecular tensor [4]. The third-order susceptibility of a low-concentration solution of molecules is then

$$\chi_{1111}^{(3)}(C) = \chi_{1111}^{(3)}(0) + f^4 \rho N_A \gamma_{\rm rot} C/M, \tag{3}$$

where $\chi_{1111}^{(3)}(0)$ is the third-order susceptibility of the solvent, ρ is the mass density of the solvent, N_A is Avogadro's number, C is the concentration of molecules expressed as the mass of the solute divided by the mass of the solution, and M is the molar mass.

The nonlinear absorption of a single optical wave is related to an intensity-dependent change in absorption constant α that can be described as

$$\alpha(I) = \alpha(0) + \beta I, \tag{4}$$

where I is the light intensity and β is the two-photon absorption coefficient. Using the third-order nonlinear polarization created through $\chi_{1111}^{(3)}(-\omega,-\omega,\omega,\omega)$ as a source term in the wave equation for a linearly polarized wave shows that [3]

$$\beta = \frac{3\omega}{2\epsilon_0 c^2 n^2} \mathrm{Im}\left[\chi_{1111}^{(3)}\right] = \frac{3\pi}{\epsilon_0 c n^2 \lambda} \mathrm{Im}\left[\chi_{1111}^{(3)}\right], \tag{5}$$

where n is the refractive index of the material in which the wave propagates and λ is the vacuum wavelength corresponding to ω. The two-photon coefficient β is related to a molecular two-photon absorption cross section σ by $\beta = N\sigma$, where N is the density of molecules. For randomly oriented molecules (i.e., in solution) σ must be understood as an orientational average. It can be expressed in terms of the imaginary part of $\gamma_{\rm rot}$ by inserting $\chi_{1111}^{(3)} = N f^4 \gamma_{\rm rot}$ [from Eq. (2)] into Eq. (5) to obtain

$$\beta = N\sigma, \tag{6}$$

$$\sigma = f^4 \frac{3\omega}{2\epsilon_0 c^2 n^2} \mathrm{Im}[\gamma_{\rm rot}], \tag{7}$$

where σ has units of m^4/W, or $\mathrm{cm}^4/\mathrm{GW}$. One often defines a two-photon absorption cross section $\sigma^p = \hbar\omega\sigma$ which is given in terms of a photon flux instead of power, and has units of $\mathrm{m}^4\,\mathrm{s}$ per photon, or of $\mathrm{GM} = 10^{-50}\ \mathrm{cm}^4\,\mathrm{s/photon}$ (GM after Göppert-Meyer [5]). Unfortunately, the molecular two-photon absorption coefficient defined in this way depends on the refractive index of a hypothesized material in which the molecules are embedded. This is one drawback of using the two-photon absorption cross section σ instead of the imaginary part of the third-order polarizability, but the prevailing use of σ in the literature prompts us to use it in this work, too.

Finally, it is useful to compare the third-order polarizability of a molecule to both the size of the molecule itself and a fundamental limit that is essentially determined by the number of conjugated electrons [6–8]. Such a comparison can be made for each molecule by deriving its intrinsic third-order polarizability γ_I [9] and its specific third-order polarizability $\tilde{\gamma}$ [10,11]. γ_I is defined as the ratio between the experimentally determined rotational average of the third-order polarizability, $\gamma_{\rm rot}$, and a value γ_K (see Sec. IV) representing the fundamental limit [9]. The specific third-order polarizability $\tilde{\gamma}$ is obtained by dividing the same experimental $\gamma_{\rm rot}$ by the mass of the molecule [10,11], and it describes the potential of obtaining large bulk third-order susceptibilities if the molecules can be combined into a dense supramolecular assembly [11–14]. Similar definitions for assessing two-photon absorption will be discussed in Sec. IV.

III. MOLECULES

The molecules studied in this work are shown in Fig. 1. They are all characterized by efficient off-resonant third-order nonlinearities [10–13,15] that have been shown to be very high compared to both the off-resonant fundamental limit and the size of the molecule.

Molecule 1—TDMEE [10]—is the smallest molecule in the series, with the highest specific and intrinsic third-order polarizability [10]. Molecule 2—DDMEBT [12,13,16]—is a variant of molecule 1 that is nonplanar and forms high

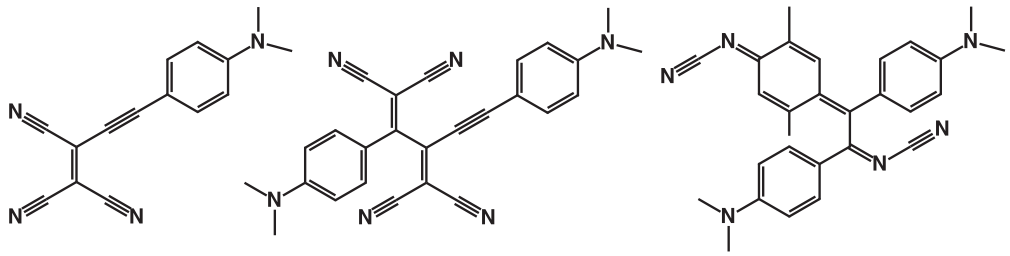

FIG. 1. Chemical structure of the molecules investigated in this work. From left to right, molecules 1 (TDMEE in Ref. [10]), 2 (DDMEBT in Ref. [12]), and 3 (3c in Ref. [15]).

quality thin films by vapor deposition [12]. Such films have been successfully used to create ultrahigh speed all-optical switches on the silicon photonics platform [17,18]. Finally, molecule 3 [15] is part of a different family. The absorption spectrum of each of these compounds is shown in Fig. 2. The double-peaked spectrum of molecule 3 is related to the fact that, in contrast to molecules 1 and 2, it has two comparable charge-transfer transitions from either of the two dimethylamino donor groups to the cyano acceptors [15]. Since all these molecules are noncentrosymmetric, the first excited state reached by linear absorption can also be reached by two-photon absorption and the wavelength of the maximum two-photon absorption in these molecules is expected to correspond to twice the peak wavelength λ_{max} for the longest wavelength linear optical absorption.

The very efficient off-resonant nonlinearities of the compounds in Fig. 1 [10,12,13,15,16], and their demonstrated significance for applications [12,17–19], motivate a more complete characterization of the behavior of their nonlinear response when the optical wavelengths start approaching the first two-photon absorption resonance.

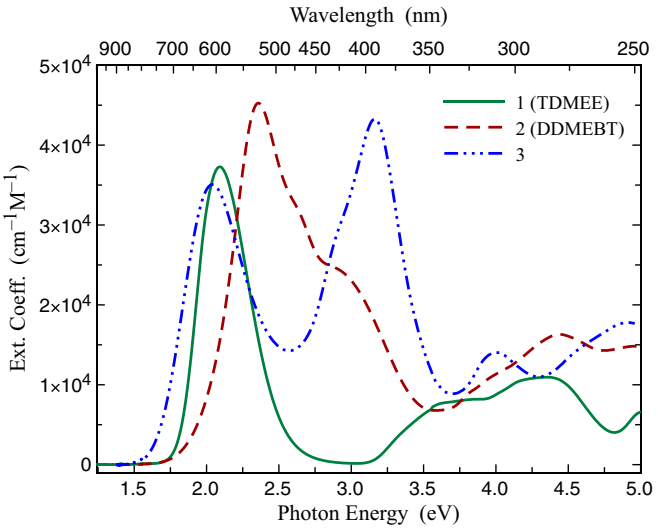

FIG. 2. (Color online) Spectrum of the linear molar extinction coefficient, in units of $cm^{-1}\,M^{-1}$, of molecules 1, 2, and 3. The excitation energies to the first optically accessible excited state, E_{10}, are 2.09, 2.36, and 2.04 eV respectively. The estimated energies representative of the next higher electronic excited state, E_{20}, are estimated to be 3.60, 4.45, and 3.16 eV.

IV. FUNDAMENTAL LIMIT FOR TWO-PHOTON ABSORPTION

A fundamental upper limit to the nonlinear optical polarizabilities of a molecule has been developed by Kuzyk [6–8,20,21]. For third-order effects, the off-resonant fundamental limit is given by the fourth power of the maximum dipole transition matrix element divided by the third-power of the first optical excitation energy E_{10} [7],

$$\gamma_k = \frac{1}{\epsilon_0}\left[\frac{e^2\hbar^2 N_\pi}{2m^2 E_{10}}\right]^2 \frac{1}{E_{10}^3} = \frac{e^4\hbar^2}{\epsilon_0 m^2}\frac{N_\pi^2}{E_{10}^5}, \tag{8}$$

where ϵ_0 is the electric constant that is part of the definition of the polarizability in the S.I. system, the term in square brackets is the square of the maximum dipole transition matrix element as determined by sum rules [7], e is the elementary charge, m is the electron mass, and N_π is the number of conjugated electrons in the molecule. Here we extend Kuzyk's derivation of a fundamental limit for resonant two-photon absorption [20] to the case of the molecules and experiments discussed in this work.

For third-order effects like self-phase modulation or degenerate four-wave mixing, two-photon absorption is the first resonant excitation encountered when raising the photon energy from the zero-frequency limit. For noncentrosymmetric molecules this is a two-photon transition to the same first excited state that is seen as a one-photon transition in linear absorption spectra. The largest term in the sum-over states expansion for the third-order polarizability that becomes resonant in this case has the form [22]

$$\gamma \propto \frac{\mu_{02}^2\mu_{12}^2}{(E_{20}-\hbar\omega-i\Gamma_{20})^2(E_{10}-2\hbar\omega-i\Gamma_{10})}, \tag{9}$$

where $\mu_{nm} = \langle n \mid \hat{p} \mid m\rangle$ is the dipole transition matrix element between state n and m, E_{i0} is the energy difference between excited state i and the ground state, and Γ_{i0} is the corresponding damping constant, responsible for a finite linewidth.

We are interested in the fundamental limit for the lowest energy two-photon absorption in a system where $E_{10} < E_{20}$ and for which a two-photon resonance occurs for a photon energy of $\hbar\omega = E_{10}/2$ (this excludes the possibility of a concurrent one-photon resonance). This description is appropriate for the noncentrosymmetric molecules studied here, but it differs from that used in Ref. [20]. It follows that we cannot directly use the results of Ref. [20] for the resonant fundamental limit, but must instead derive the appropriate expression for the case of

a two-photon transition that goes from the ground state to the lowest energy excited state.

Following Kuzyk [20], we start by considering the difference between resonant and off-resonant values of the term in Eq. (9). Assuming $(E_{20},E_{10}) \gg (\Gamma_{20},\Gamma_{10})$, the ratio between the imaginary part and the real part of Eq. (9) in the zero-frequency limit is

$$\frac{\mathrm{Im}[\gamma_0]}{\mathrm{Re}[\gamma_0]} = \frac{\Gamma_{10}}{E_{10}} + 2\frac{\Gamma_{20}}{E_{20}}, \tag{10}$$

and the ratio between the imaginary parts of resonant and off-resonant third-order polarizabilities is

$$\frac{\mathrm{Im}[\gamma^{\mathrm{res}}]}{\mathrm{Im}[\gamma_0]} = \left[\frac{E_{20}}{E_{20}-E_{10}/2}\right]^2\left[\frac{\Gamma_{10}}{E_{10}}\right]^{-1}\left[2\frac{\Gamma_{20}}{E_{20}}+\frac{\Gamma_{10}}{E_{10}}\right]^{-1}. \tag{11}$$

Multiplying Eq. (10) with Eq. (11) gives the ratio between the peak imaginary part at resonance and the off-resonant real part,

$$R = \frac{\mathrm{Im}[\gamma^{\mathrm{res}}]}{\mathrm{Re}[\gamma_0]} = \frac{E_{10}E_{20}^2}{(E_{20}-E_{10}/2)^2\,\Gamma_{10}}. \tag{12}$$

It is worth pointing out at this stage that, even though this ratio applies to the case of a two-photon resonance at $\hbar\omega = E_{10}/2$, we prefer to not make this substitution in Eq. (12) and all the other expressions derived below. This avoids giving them the appearance of frequency-dependent quantities, which they are not.

Since the ratio (12) is also valid for the case where the third-order polarizability is at its fundamental limit, one can obtain a fundamental limit for the peak imaginary part on-resonance by multiplying R with the fundamental off-resonant limit γ_K [see Eq. (8)]. The final result for the fundamental upper limit to the imaginary part of the third-order polarizability on the peak of the two-photon resonance ($\hbar\omega = E_{10}/2$) is then

$$\mathrm{Im}\left[\gamma_k^{\mathrm{res}}\right] = \gamma_k R = \gamma_k \frac{E_{10}}{\Gamma_{10}}\left[1-\frac{1}{2}\frac{E_{10}}{E_{20}}\right]^{-2}, \tag{13}$$

where we have rewritten the ratio R of Eq. (12) to highlight the fact that $E_{10}/\Gamma_{10} < R < 4E_{10}/\Gamma_{10}$. Thus, the fundamental limit to the imaginary part of γ on resonance is essentially given by the off-resonant limit multiplied by the ratio between the resonance energy and the linewidth (this corresponds to the value reached when the second excited state is far away from the first excited state). The limit can then become four times larger when the excited states have energies close to each other.

Inserting Eq. (13) for $\mathrm{Im}[\gamma_{\mathrm{rot}}]$ into Eq. (7) delivers the fundamental limit σ_K (or $\sigma_K^p = \hbar\omega\sigma_K$) to the two-photon absorption cross section:

$$\sigma_K^p = \gamma_k f^4 \frac{3}{2\hbar\epsilon_0 c^2 n^2}\left[\frac{E_{10}}{2}\right]^2\frac{E_{10}}{\Gamma_{10}}\left[1-\frac{1}{2}\frac{E_{10}}{E_{20}}\right]^{-2}, \tag{14}$$

where we used $\hbar\omega = E_{10}/2$ on the peak of the two-photon resonance. Note that in both Eqs. (13) and (14), γ_K from Eq. (8) contains a factor $1/E_{10}^5$, which, when the first and second excited states are far away from each other, implies that σ_K^p is inversely proportional to the square of E_{10} (while σ_K and $\mathrm{Im}[\gamma_K^{\mathrm{res}}]$ are inversely proportional to the third and fourth powers of E_{10}, respectively).

The result of Eqs. (13) and (14) follows the treatment in Ref. [20], but we repeat that in the present derivation we assumed two-photon absorption to the *lowest* of the two states, i.e., the case of $\hbar\omega = E_{10}/2$ and $E_{10} < E_{20}$, while Ref. [20] calculated instead the fundamental limit for a two-photon transition to the *upper* state. The absence of the possibility of a double resonance in our result is a reflection of the condition that $E_{20} > E_{10}$, which keeps the denominator in Eqs. (13) and (14) positive and far from zero. Instead, the equivalent expression in Ref. [20] has a pole for $E_{20} = 2E_{10}$ [20].

V. DEGENERATE FOUR-WAVE MIXING

In this section we review the dependence of the DFWM signal on the third-order susceptibility under conditions where either linear absorption or two-photon absorption start to affect the results. This is important when using DFWM for spectroscopy, which requires us to properly assess the effects of linear and nonlinear absorption when the wavelength approaches a two-photon resonance or the onset of linear absorption.

The complex amplitude $P^{(3)}(\omega,\mathbf{k})$ of the nonlinear optical polarization responsible for the DFWM signal is

$$P_i^{(3)}(\omega,\mathbf{k}_4) = \frac{3}{2}\epsilon_0 \sum_{j,k,l}\chi_{ijkl}^{(3)}E_j(\mathbf{k}_1)E_k(\mathbf{k}_2)E_l(\mathbf{k}_3)^*, \tag{15}$$

where the $E_j(\mathbf{k}_n)$ are the amplitudes of the three interacting fields (the "pump" waves) with different wave vectors, the superscript asterisk denotes complex conjugation, ϵ_0 is the electric constant, and we define the time-dependent fields $E_j(\mathbf{r},t)$ as the real part of $E_j(\mathbf{k}_n)\exp(i\mathbf{k}_n\cdot\mathbf{r}-i\omega t)$. The wave vector of the third-order polarization is $\mathbf{k}_4 = \mathbf{k}_1+\mathbf{k}_2-\mathbf{k}_3$.

In the following we calculate the DFWM signal strength when the three pump waves suffer from either linear or nonlinear absorption, leading to a dependence of their amplitude from the propagation distance inside the sample.

We first consider the case of linear absorption, for which the amplitudes of the pump waves have a spatial dependence given by $E_j(\mathbf{k}_n,z) = E_j^0(\mathbf{k}_n)\exp(-\alpha z/2)$, where α is the linear absorption constant. In a DFWM experiment where the three interacting beams enter the sample from the same side with a small angle between each other, the z dependence of the induced third-order polarization is $P^{(3)}(z) = P^{(3)}(0)\exp(-3\alpha z/2)$. Inserting this polarization as a source term into the wave equation, and using the slowly varying amplitude approximation to eliminate second-order space derivatives, results in

$$2ik_4\frac{\partial}{\partial z}E_4(z) - k_4^2E_4(z) + \frac{\omega^2n^2}{c^2}E_4(z) + ik_4\alpha E_4(z) = -\frac{\omega^2}{c^2}\frac{3}{2}\chi^{(3)}E_1E_2E_3^*e^{-3\alpha z/2}, \tag{16}$$

where E_4 is the amplitude of the radiated signal wave. For a phase-matched four-wave mixing configuration with the wave vector of the radiated wave equal to the wave vector of the

third-order polarization, this equation simplifies to

$$\frac{\partial}{\partial z}E_4(z) = i\frac{k_4}{2n_4^2}\frac{3}{2}\chi^{(3)}E_1E_2E_3^*e^{-3\alpha z/2} - \frac{\alpha}{2}E_4(z), \quad (17)$$

which can be solved for $E_4(z)$ to give

$$E_4(z) = -i\frac{k_4}{2n_4^2}\frac{3}{2}\chi^{(3)}E_1E_2E_3^*\left[\frac{1-e^{-\alpha z}}{\alpha}e^{-\alpha z/2}\right]. \quad (18)$$

It follows that the intensity of the radiated signal wave depends on the intensity of the three pump waves and on the interaction distance z as

$$I_4 \propto \frac{z^2}{n_1n_2n_3n_4}I_1I_2I_3\left|\frac{3}{2}\chi^{(3)}\right|^2A^2, \quad (19)$$

where here $A = A_\alpha$ and

$$A_\alpha = \frac{1-e^{-\alpha z}}{\alpha z}e^{-\alpha z/2} \quad (20)$$

is an attenuation factor. A_α^2 tends to $(1-2\alpha z)$ for $\alpha z \to 0$, and can also be well approximated by $\exp(-2\alpha z)$. For a sample of thickness z, this is equivalent to saying that the signal intensity I_4 is proportional to $z^2I_1I_2I_3$ with all intensities taken in the middle of the sample. An example of the prediction of Eqs. (19) and (20) is shown in Fig. 3 (dashed curves). The DFWM signal amplitude reaches a maximum for $\alpha z = \ln(3)$, when the linear transmission through the sample equals 1/3, and then falls to zero as the thickness increases and more and more linear losses occur.

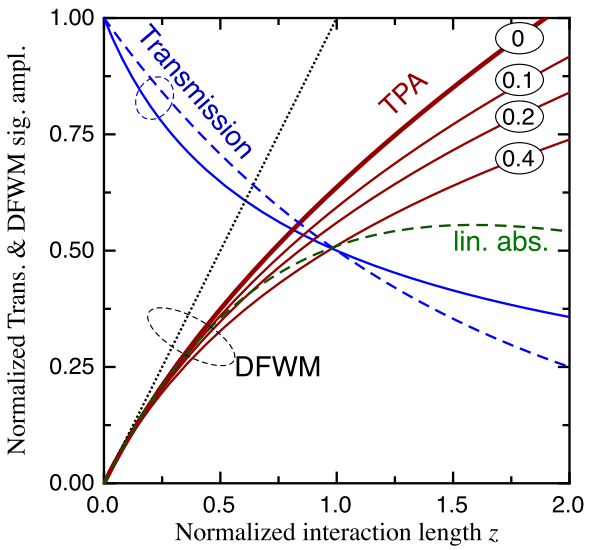

FIG. 3. (Color online) Comparison of the relative effects of different pump beam depletion mechanisms on the growth of the amplitude of the DFWM signal with interaction length z. The dashed curves are for the case of linear absorption, the solid curves are for the case of two-photon absorption, and z is normalized in such a way that the transmission in both cases becomes 0.5 at $z = 1$. The figure shows both the z dependence of the transmittivity of a pulse (curves labeled "Transmission"), and the corresponding z dependence of the DFWM signal amplitude (curves labeled "DFWM"). The dotted line is the linear z dependence of the DFWM signal amplitude that occurs in the absence of any pump depletion. The labels on the solid curves for the DFWM signal amplitude give the ratio between the two pump pulses with the highest intensity in the case where the third pump pulse is negligibly weak. The curve labeled "0" corresponds to the square root of Eq. (19) with A given by Eq. (31). The curves with labels 0.1-0.2-0.4 are obtained by numerical integration of Eq. (28).

Next, we consider the case of pump waves that are affected by two-photon absorption, which leads to an attenuation of light intensity described by $dI(z)/dz = -\beta[I(z)]^2$, where β is the two-photon absorption coefficient. The resulting space dependence of the intensity is

$$\frac{I(z)}{I(0)} = \frac{1}{1+\beta I(0)z}. \quad (21)$$

In a practical experiment, the intensity $I(0)$ that is incident on a sample is modulated in both space and time. We assume a collimated beam with a Gaussian spatial and temporal intensity-profile (beam waist w_0, pulse duration τ) described by

$$I(z=0,r,t) = I_0e^{-2r^2/w_0^2-t^2/\tau^2}, \quad (22)$$

where r is the lateral distance from the beam axis and I_0 is the peak intensity, given by

$$I_0 = \frac{2}{\pi^{3/2}w_0^2\tau}E_p(0), \quad (23)$$

where $E_p(0)$ is the experimentally determined pulse energy incident on the sample. The pulse energy after a propagation distance z is obtained by integrating the intensity given by (21) over space and time [23],

$$E_p(z) = \int_{-\infty}^{\infty}\int_0^{\infty}2\pi r\frac{I(r,t)}{1+\beta I(r,t)z}drdt \quad (24)$$

$$= \frac{\pi w_0^2}{2\beta z}\int_{-\infty}^{\infty}\ln\left[1+\beta I_0ze^{-t^2/\tau^2}\right]dt, \quad (25)$$

from which one can define a nonlinear transmittivity $T_{NL} = E_p(z)/E_p(0)$:

$$T_{NL} = \frac{1}{\sqrt{\pi}\beta I_0z\tau}\int_{-\infty}^{\infty}\ln\left[1+\beta I_0ze^{-t^2/\tau^2}\right]dt. \quad (26)$$

It is useful to note that for a continuous wave (cw) collimated Gaussian beam the equivalent expression for the nonlinear transmittivity would be [23]

$$T_{NL}^{(cw)} = \frac{1}{\beta I_0^{(cw)}z}\ln\left[1+\beta I_0^{(cw)}z\right], \quad (27)$$

where $I^{(cw)} = 2P^{(cw)}/(\pi w_0^2)$, with $P^{(cw)}$ the beam power. As long as the transmittivity does not become too small, Eq. (27) can be used for a pulsed laser as a simpler approximation to Eq. (26) if one substitutes $I_0^{(cw)} = 0.7I_0$, where I_0 is the peak intensity (23) of the pulse. One can show that this delivers a nonlinear transmittivity too small by only ~5% when reaching an attenuation $T_{NL} = 0.5$. Similarly, one can also show that even the simple expression (21) can approximate Eq. (26) with the substitution $I(0) = 0.35I_0$, but this approximation breaks down earlier, giving a transmission too small by 5% already for $T_{NL} = 0.75$. When calculating the nonlinear transmission for a collimated pulsed beam we will later use Eq. (27) with $I_0^{(cw)} = 0.7I_0$.

For DFWM experiments with three pump beams, nonlinear absorption as described above leads to an interaction length between the pump waves that is shorter than the sample thickness, and to a DFWM signal that becomes saturated at higher pump intensities, higher nonlinear absorption, or thicker samples. By neglecting the influence of pump beams on each other, one can approximate the evolution of the signal wave amplitude, in a simple plane-wave approximation, by using Eq. (21) to obtain the spatial profile of the nonlinear polarization responsible for the DFWM signal (nonlinear absorption will be irrelevant for the generated signal wave, which has a much lower intensity). The resulting wave equation would be

$$\frac{\partial}{\partial z}E_4(z) = i\frac{k_4}{2n^2}\frac{3}{2}\chi^{(3)}E_1E_2E_3^* \times\left[\frac{1}{(1+\beta I_1 z)(1+\beta I_2 z)(1+\beta I_3 z)}\right]^{1/2}, \quad (28)$$

where the I_i are the intensities of the three "pump" beams that create the nonlinear polarization. But it is worth repeating that when the three intensities are similar, this does not take into account cross-interaction effects between the three beams. A more complete analysis would require to model the full space and time dependence of the laser pulses and their nonlinear interaction. We consider instead a situation where one of the three pump beams has an intensity significantly larger than the others. In such a case the DFWM signal is affected only by the attenuation of the strongest beam. This can be modeled using

$$\frac{\partial}{\partial z}E_4(z) = i\frac{k_4}{2n^2}\frac{3}{2}\chi^{(3)}E_1E_2E_3^*\left[\frac{1}{(1+\beta I_3 z)}\right]^{1/2}, \quad (29)$$

which has the analytical solution

$$E_4(z) = i\frac{k_4}{2n^2}\frac{3}{2}\chi^{(3)}E_1E_2E_3^*[\sqrt{1+\beta I_3 z}-1]\frac{2}{\beta I_3}. \quad (30)$$

The corresponding expression for the DFWM signal intensity is then again given by Eq. (19), but with

$$A = A_{TPA}^{I_3\gg I_1,I_2} = \frac{2(\sqrt{1+\beta I_3 z}-1)}{\beta I_3 z}. \quad (31)$$

The square of this factor tends to $1-\beta I_3 z/2$ for $\beta I_3 z \ll 1$, and in this case (31) can be well approximated by (21) taken at a distance $z/2$, which again means that when nonlinear absorption is low the DFWM signal intensity I_4 is proportional to $z^2 I_1 I_2 I_3$ with all intensities taken in the middle of the sample, similar to the case of linear absorption. An example of the prediction of Eqs. (19) and (31) is shown in Fig. 3 (solid curves).

Figure 3 highlights how the effect of nonlinear attenuation on the DFWM signal is qualitatively different from that of linear absorption, which causes a much stronger depletion of the DFWM signal amplitude as the thickness of the sample increases. There are two reasons for this. One is that nonlinear absorption does not affect the weak signal beam and therefore only influences the pump beams, while linear absorption also directly causes depletion of the signal beam. The other is that the depletion of the pump beams caused by nonlinear absorption is accompanied by a corresponding enhancement of the DFWM signal, which is always proportional to the absolute value of the third-order susceptibility [Eq. (19)]. The two effects work against each other, and the DFWM signal amplitude still keeps growing (albeit in a strongly sublinear way) when the imaginary part of the third-order susceptibility becomes very large or when nonlinear attenuation becomes extreme at high intensities. This can be clearly seen by inserting (31) into (19) and noticing that in the limit of large β when the imaginary part of the third-order susceptibility dominates and when $\beta I_3 z \gg 1$, the DFWM signal intensity becomes independent from I_3 and proportional to β (while it would be proportional to $|\beta|^2$ when the imaginary part of the third-order susceptibility is dominant but $\beta I_3 z \ll 1$).

Figure 3 also explores the regime of validity of Eqs. (19) and (31), which can be assessed by comparing their prediction with the result of a numerical integration of (28), the next better, if imperfect, approximation. This is done in Fig. 3 for $I_1 \ll I_2$ and different ratios I_2/I_3 between 0.0 and 0.4. The figure shows that the simpler expression (31) already gives a useful picture of the effect of nonlinear absorption. But for sample thicknesses such that the strongest pump beam is attenuated by 50%, Eq. (31) gives a DFWM signal amplitude too high by ~10% already when $I_2 = 0.2I_3$ (while keeping I_3 constant and $I_1 \ll I_2$). It follows that under circumstances of significant nonlinear attenuation the use of (31) should be limited to experiments where I_3 is at least five times larger than the intensities of the other two pump beams. Finally, we note that we will use (31) only to model how an increase in β will cause a *relative deviation* of the DFWM signal amplitude from its value in the absence of nonlinear attenuation (see later), but not to model the absolute value of the DFWM signal itself. It is therefore not necessary, in this context, to precisely evaluate how the intensity I_3 used in (31) relates to the actual peak intensity of a pulsed beam.

VI. EXPERIMENT

We use 1-ps duration light pulses [described by Eq. (22) with $\tau = 0.43$ ps] at a repetition rate of 1 kHz, obtained from a Light Conversion TOPAS (traveling-wave optical parametric amplifier system) pumped by a Clark-MXR CPA 2101 laser. For most of the experiments presented here, we use the signal wave of our TOPAS, tuning its wavelength between 1080 and 1680 nm.

We perform DFWM experiments using the forward configuration depicted in Fig. 4, with the components of the interacting wave vectors in the plane of the sample positioned at the opposite corners of a square for beam 1 and 2, and in one of the other corners for beam 3. The wave vector of the DFWM signal (beam 4) then points to the remaining corner. As mentioned above, we taylor our DFWM experiments to realize the case where nonlinear absorption remains a small perturbation that can be well approximated by Eqs. (29) and (31), even near two-photon resonances. We do this by choosing the intensity of beam 3 to be much larger than that of the other beams. We then simultaneously monitor both the energy of the DFWM signal pulse as well as the transmission of beam 3 through the sample. Since the strongest beam will be the first to experience the effects of nonlinear absorption, beam 3 essentially serves as a "canary in the gold mine"

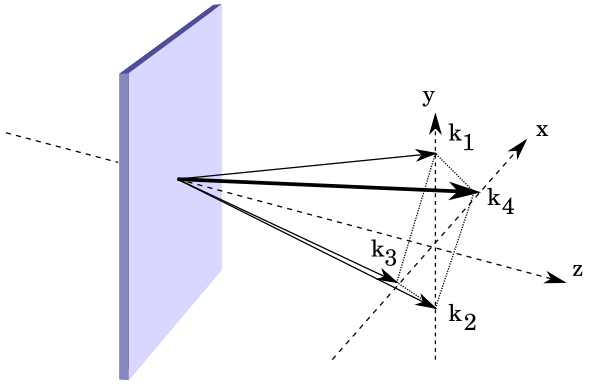

FIG. 4. (Color online) Illustration of the forward DFWM geometry used in this work. The incident beams with wave vectors $\mathbf{k}_1$, $\mathbf{k}_2$, and $\mathbf{k}_3$ overlap in the sample in such a way that the third-order nonlinear optical polarization they induce radiates a signal beam with wave vector $\mathbf{k}_4 = \mathbf{k}_1 + \mathbf{k}_2 - \mathbf{k}_3$ in a phase-matched way.

to alert that the DFWM signal can be depleted because of nonlinear absorption of the pump waves. The data from the transmission of beam 3 therefore serves to model and control the onset of two-photon-induced attenuation of the DFWM signal, and close to a resonance it provides additional data on the imaginary part of the third-order susceptibility and its wavelength dependence.

All beams are focused by 1-m focal length lenses to a beam waist of $\sim$110 μm (at 1180 nm). The arrival times of the pulses in the sample are controlled by translation stages. When pulse 1 is delayed with respect to the others, the DFWM signal is sensitive to any population grating left behind by the interference of pulses 2 and 3, a fact that can be used to observe the dynamics of excited states, including those created by two-photon absorption. For all samples and wavelengths investigated here, the DFWM signal obtained when all pulses passed through the sample at the same time was always more than 100 times larger than any remnant signal obtained when the third pulse was delayed by a few pulse durations and diffracted off the grating written by the two other pulses.

Compared to other experimental techniques that are sensitive to the third-order susceptibility, DFWM offers several advantages, such as a backgroundless signal, better sensitivity at low intensities (allowing experiments using weakly focused beams), and the ability to observe excited-state absorption and excited-state lifetimes by delaying one of the three interacting pulses. In addition, in a DFWM experiment the imaginary part of the third-order susceptibility can contribute significantly to the detected signal, as described by $|\chi^{(3)}|^2$, without causing any signal depletion as long as $\beta I z \ll 1$ (see the previous section). In such a case the only direct effect of an imaginary part of the susceptibility in DFWM is an additional phase shift of the generated signal wave. This is different than for, e.g., Z scan, where the imaginary part of the third-order susceptibility is necessarily given by the attenuation of the transmitted wave [24].

We determine the wavelength dependence of molecular third-order polarizabilities by measuring the third-order susceptibilities of molecular solutions with different concentrations at different wavelengths and modeling the results to separately extract the real and imaginary part of the third-order polarizability.

The solutions are prepared in $d = 1$-mm-thick fused silica spectroscopy cells. The solvent is dichloromethane (CH_2Cl_2, DCM), with refractive index $n = 1.42$ and density $\rho = 1.3266$ g/cm^3. The third-order susceptibility of the solution is described by Eq. (3). Absolute values for the third-order susceptibility of the solutions are obtained by comparing their DFWM signal to that obtained in a reference measurement that established the $\chi^{(3)}_{1111}(0)$ for a 1-mm cell filled with the pure solvent to be 6 ± 1 times larger than for a 1-mm-thick fused silica sample, for which we used a third-order susceptibility of 1.9×10^{-22} m^2 V^{-2}. This fused-silica value corresponds to the weighted average of the values given in Refs. [25–28] taking into account dispersion, as well as the different nonlinear processes used in the different references. All values used in the average are within 10% of each other.

At wavelengths such that no linear or nonlinear absorption takes place ($\beta I d \ll 1$), the third-order susceptibility of the solution is obtained from the ratios between the DFWM signal at a given concentration and at zero concentration, $|\chi^{(3)}_{1111}(C)|/\chi^{(3)}_{1111}(0)$, and Eq. (19) with $A = 1$. When linear absorption starts to slightly deplete the pump waves responsible for the DFWM signal, we use Eq. (19) with A given by Eq. (20). Near two-photon resonances, when the concentration of molecules or the intensity are so high that $\beta I d$ starts becoming comparable to 1, we extract $|\chi^{(3)}_{1111}(C)|$ from the data by using Eq. (19) with A given by Eq. (31).

The concentration dependence of the DFWM signal amplitude is determined by the concentration dependence of the third-order susceptibility via (3), and it is linear with concentration as long as the third-order polarizability of the dissolved molecules is real-valued. But since the molecular contribution to the third-order susceptibility adds coherently to the real-valued third-order susceptibility of the solvent, the concentration dependence of $|\chi^{(3)}_{1111}(C)|/\chi^{(3)}_{1111}(0)$ becomes nonlinear as a two-photon resonance is approached. This allows us to obtain both the real and imaginary part of $\gamma_{\rm rot}$ by fitting Eq. (3) to the data. At higher intensities or concentrations, nonlinear attenuation becomes detectable on the transmission of beam 3, and the corresponding data, modeled with Eqs. (27) and (6) and (7), can also be taken into account to improve the accuracy of the imaginary part of $\gamma_{\rm rot}$ and its wavelength dependence.

An example of DFWM and nonlinear transmission data, collected at four intensities in the region where two-photon absorption starts to affect the pump pulses, is shown in Fig. 5 for molecule 1. At the wavelength of 1180 nm used in this experiment the third-order polarizability has a large positive imaginary part and a large negative real part. The DFWM signal obtained in the solution is normalized to the signal at zero concentration and its square root is plotted as a function of concentration in the top panel. The data for the transmission of beam 3 collected at the same concentrations is given in the bottom panel. The whole data set can be modeled using the procedure described above, involving Eq. (3), Eq. (19) with A given by Eq. (31), Eq. (27), and Eqs. (6) and (7). The different curves in the top panel of Fig. 5 give the results of a fit of the model to the DFWM data for every intensity,

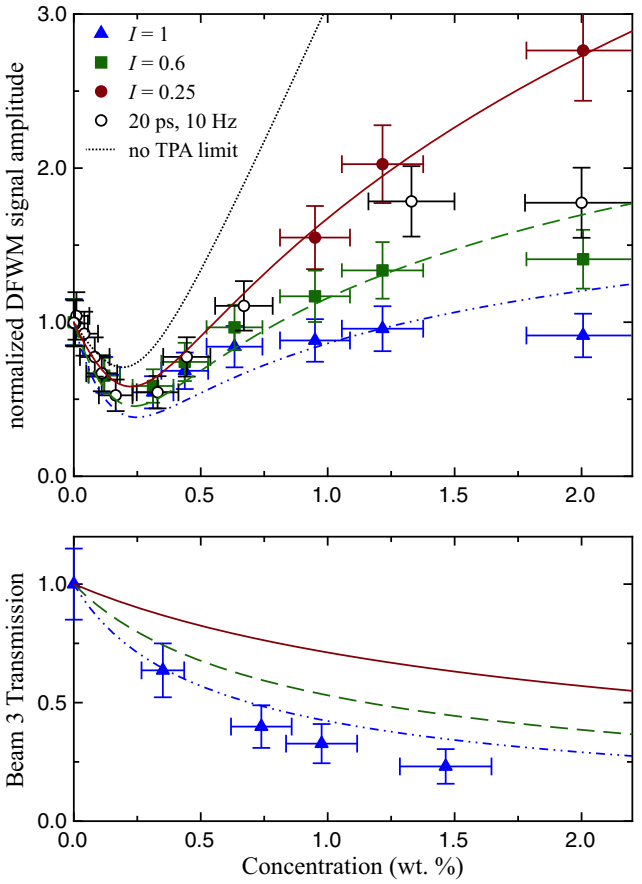

FIG. 5. (Color online) Concentration dependence of DFWM signal amplitude and transmission measured near the two-photon resonance (wavelength of 1180 nm) of molecule 1 for a range of intensities where two-photon-induced attenuation of the pump waves is significant. Top panel: Experimental DFWM signal amplitude obtained in a 1-mm-thick solution at different molecular concentrations and four different pump intensities. Normalized relative intensities are given in the legend for three of the data sets. The highest intensity corresponded to $\sim 10^{15}$ W/m^2. The data set represented by the open circles was obtained in a completely different setup using a 10-Hz repetition rate and 20-ps-long pulses, but gives essentially the same concentration dependence as the other experiments. The data points are accompanied by the result of a simultaneous least-squares fit with Eqs. (28) and (3) that delivered $\gamma_{\rm rot} = [(-31 \pm 5) + i(29 \pm 5)] \times 10^{-48}$ m^5 V^{-2}. Bottom panel: Transmission of the strongest individual pump beam (I_3), measured simultaneously with the DFWM signal displayed in the upper panel. Only the data set taken at the highest intensity is shown. The curves are obtained from Eq. (27) using the same parameters that fit the DFWM data in the upper panel and the experimental intensity. The highest intensity curve is compatible with the data within the error bars.

while the prediction of the same model for the transmission of beam 3 is given in the bottom panel. In the limit where two-photon-induced attenuation is not important, the square root of the DFWM signal is proportional to the absolute value of the third-order susceptibility of the solution. In the experiment of Fig. 5, the DFWM signal is clearly more and more attenuated as the concentration of the molecule and the imaginary part of the third-order susceptibility of the solution increase (such an attenuation can be avoided in an experiment using either thinner solutions or less focused beams). But the model can take this into account fairly well, especially at lower concentrations and lower intensities. In addition, the prediction of the same model matches well the experimental transmission data that was measured at the highest intensity (bottom panel in the figure), demonstrating that the attenuation of the DFWM signal at higher concentrations and higher intensities is indeed related to the decrease in transmission caused by two-photon absorption, plotted in the bottom panel.

The fitted values for Re[$\gamma_{\rm rot}$] and Im[$\gamma_{\rm rot}$] obtained from the DFWM data in Fig. 5 agree with the other measurements that will be presented below. We also note that in the low intensity limit the real part of the third-order susceptibility of the solution becomes negative for concentrations higher than $\sim$0.35% when Re[$\gamma_{\rm rot}$] $\sim -30 \times 10^{-48}$ m^5 V^{-2}. The negative susceptibility leads to self-defocusing, which we confirmed by a Z-scan experiment performed at the resonant two-photon absorption wavelength [29].

The methodology explained above can be used to analyze data that are acquired in an automatic wavelength scan to obtain a spectrum of both the real and the imaginary part of the third-order polarizability. To do this, we prepare seven identical spectroscopy cells containing seven different concentrations in the range from 0% up to $\sim$2% concentration in mass. Then, each of the seven cells is used in a DFWM experiment where the wavelength of the interacting beams is automatically scanned while data are collected, taking care not to change anything in the adjustment of the experiment when moving from one concentration to the next. As long as pump beam attenuation caused by two-photon absorption is not significant (limit of thin samples and low intensity), the relative ratios between the DFWM signals obtained at different concentrations (including zero concentration) are insensitive to variations in laser output power, or to slight misadjustments of the setup, that occur while the wavelength is scanned over the wavelength interval of interest. This is the important feature of the DFWM measurement that allows for computer-controlled scanning of wavelength and capturing of data without operator intervention.

The details of the measurement program are as follows. During a typical computer-controlled wavelength scan, the data acquisition program scans the wavelength emitted by the TOPAS over the range between 1080 and 1680 nm. Concurrently, it controls the delay time Δt between pulse 1 and the other pump pulses and collects the DFWM signal at each wavelength both for $\Delta t = 0$ and for $\Delta t = -1.5$ ps, when pump pulse 1 reaches the sample more than one pulse width *before* the other two pump pulses. The strength of the DFWM signal is obtained from the difference between the measurement taken at $\Delta t = 0$ and the measurement taken at $\Delta t = -1.5$ ps, which eliminates any effect from drifts of signal background. In addition, the energy of pulse 3 transmitted by the sample is also measured. Both the DFWM signal and the transmission signal as a function of wavelength and concentration are stored for subsequent analysis.

The numerical analysis of the data is based on a multidimensional least-squares fit of the data using a model that predicts both the DFWM signal strength and the transmission of beam 3 from the wavelength-dependent real and imaginary part of the

third-order polarizability. While we have already described all the calculations required to do this, we repeat here the full set of equations used for the analysis. Starting from the third-order polarizability, we arrive at the two measured quantities: T_3, the transmission of pump beam 3 through the sample, and $S = \sqrt{I_4(C)/I_4(0)}$, the square root of the ratios between the DFWM signals for a solution with mass concentration C and for the pure solvent,

$$\chi^{(3)}_{1111} = \chi^{(3)}(0) + f^4 \rho N_A \gamma_{\rm rot} C/M, \tag{32}$$

$$\beta = \frac{3\pi}{\epsilon_0 c n^2 \lambda} \mathrm{Im}\left[\chi^{(3)}_{1111}\right], \tag{33}$$

$$A_\alpha = \frac{1 - e^{-\alpha z}}{\alpha z} e^{-\alpha z/2}, \tag{34}$$

$$A_{TPA} = \frac{2(\sqrt{1 + \beta I_3 z} - 1)}{\beta I_3 z}, \tag{35}$$

$$T_3 = \frac{\ln[1 + \beta I_3 d]}{\beta I_3 d}, \tag{36}$$

$$S = \left| \frac{\chi^{(3)}_{1111}}{\chi^{(3)}(0)} \right| A, \tag{37}$$

where $A = A_{TPA}$ is used in wavelength ranges where two-photon-induced nonlinear attenuation of the pump beams is known to take place, and $A = A_\alpha$ is used at shorter wavelengths where linear absorption starts having an effect. If the linear absorption is due to the diluted molecules, then the absorption constant can be directly calculated from $\alpha = \ln(10)\varepsilon\rho C/M$, where ε is the extinction coefficient. I_3 is calculated as 0.7 times the result of Eq. (23), which is determined from the beam waist of beam 3 at the sample and the corresponding pulse energy.

The above set of equations determines the experimental DFWM signal (S) and the experimental transmission of beam 3 (T_3) from the real and imaginary part of the rotational average of the third-order polarizability $\gamma_{\rm rot}$. A least-squares fit of the predicted S and T_3 to the wavelength-dependent data then delivers the wavelength dependence of $\gamma_{\rm rot}$, which is represented by two smoothly varying adjustable functions of the wavelength for the real and the imaginary part, respectively. To allow maximum flexibility, the two smoothly varying functions are defined using a Bezier curve with N control points, giving a total of $2N$ fitting parameters. We find that the best compromise between smoothing out random noise in the data and having enough resolution to describe the wavelength dependence is obtained for N between 10 and 12 for our wavelength interval between 1080 and 1680 nm. The fit is also facilitated by the fact that for the noncentrosymmetric molecules we investigated the functional form of the imaginary part of the third-order polarizability, due to two-photon absorption, can be expected to follow, at half the photon energy, the lowest energy peak of the linear absorption. The final results of the analysis are two curves describing the dispersion of $\gamma_{\rm rot}$, and the associated errors of the fitting parameters.

Figure 6 shows a plot of the wavelength-dependent third-order polarizability as obtained in this way for molecule 1.

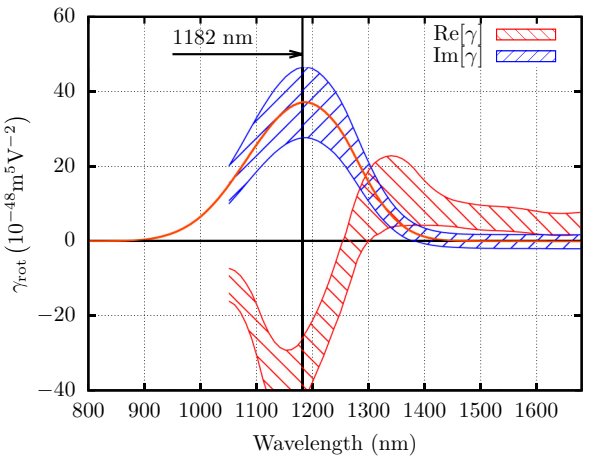

FIG. 6. (Color online) Spectrum of the third-order polarizability $\gamma_{\rm rot}$ in molecule 1 (TDMEE) as obtained from the DFWM data in a wavelength region that includes both zero-frequency limit and the first two-photon resonance. The solid line that overlaps with the band representing the allowed values for the imaginary part of $\gamma_{\rm rot}$ is a plot of the linear absorbance taken at twice the wavelength, and scaled to fit the imaginary part of $\gamma_{\rm rot}$.

In this and in other plots presented later, the spectra that are extracted from the data are given by ribbonlike bands whose vertical extension represents the experimental uncertainty.

The result in Fig. 6 shows an imaginary part of the third-order polarizability that follows the expected trend predicted by the linear absorption at twice the energy. The real part, on the other hand, is basically free from resonance enhancement as the energy approaches the two-photon transition from the zero-frequency limit. There is the possibility of a small enhancement of the positive real part of $\gamma_{\rm rot}$ around 1300 nm, but it is within the experimental error. The main effect that we observe is for the real part to start *decreasing* from its zero-frequency value as the photon energy approaches the two-photon resonance, and then to go strongly negative, reaching its largest negative value at a wavelength slightly shorter than the peak of the imaginary part.

To confirm the results obtained with this method based on DFWM, we also investigated the wavelength dependence of the imaginary part of the third-order polarizability of molecule 1 using additional experiments that are directly sensitive to the amount of two-photon absorption.

The first such experiment is simply the measurement of the transmission of a single pulse through the sample as a function of intensity and/or concentration, as presented in Fig. 5 (lower panel). The imaginary part of $\gamma_{\rm rot}$ can be extracted by fitting Eq. (36) to the data to obtain the concentration dependent two-photon absorption cross section $\beta(C)$, which is related to the imaginary part of $\chi^{(3)}$ by Eq. (33). Such data are already incorporated in the fitting procedure that delivered the result in Fig. 6. Both the amount of nonlinear transmission and its wavelength dependence is consistent with the plot in Fig. 6.

Another experiment that is highly sensitive to the amount of two-photon absorption is the detection of the amplitude of laser-induced ultrasound using a transient grating variant of DFWM. In this experiment, when molecules that have been brought into an excited state by two-photon absorption

relax back to the ground state rapidly and nonradiatively, they lead to a sudden heating of the liquid, predominantly in the regions of maximum intensity in the interference pattern. This in turn leads to thermal expansion and the later establishment of a spatially modulated strain pattern that will then oscillate elastically as an ultrasound wave [30–32]. The corresponding refractive index modulation causes Bragg diffraction of the delayed third pulse in DFWM. A measurement of the strength of this Bragg diffraction in a pump and probe measurement is a natural extension of DFWM, with the only requirement being that the probe pulse must be delayed by several nanoseconds, the time required to establish a strain pattern. We have used a second DFWM setup equipped with a longer delay track for one of the beams to measure the time dependence of the diffraction efficiency caused by the oscillating ultrasound standing wave in a solution of molecule 1. The result of a typical measurement is shown in the inset of Fig. 7. By keeping the energy of the pulses constant while changing the wavelength, we obtained the relative variation in the density of photoexcited molecules from the amplitude of the ultrasound wave detected by DFWM (which is proportional to the square root of the peak diffraction efficiency). From this, we derive the wavelength dependence of the two-photon absorption coefficient for the solution [29]. The data obtained in this way are shown as triangles in Fig. 7, and it matches the wavelength dependence of the imaginary part of the third-order polarizability that was determined in DFWM experiments. We

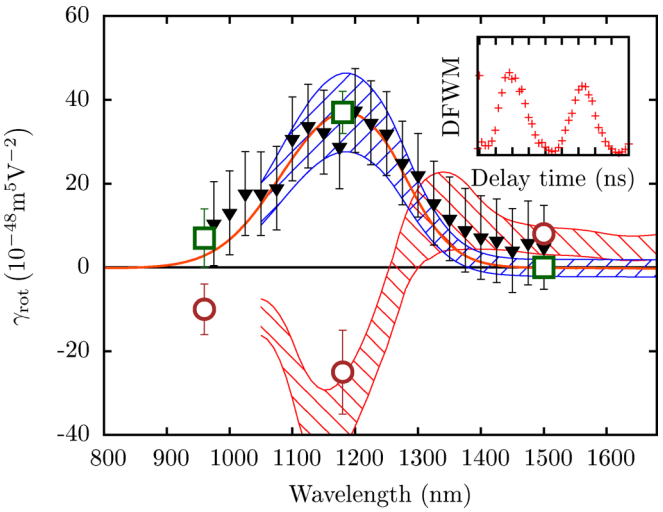

FIG. 7. (Color online) Spectrum of the third-order polarizability of molecule 1 (TDMEE), as collected from several independent experiments using different methods. The dashed ribbons are from Fig. 6. The small black triangles where obtained from the amplitude of laser-induced ultrasound (the inset gives the time dependence of the amplitude of the laser-induced ultrasound wave as detected by a transient grating experiment). The large hollow data points are the real (circles) and imaginary (squares) parts of the third-order polarizability as obtained in individual DFWM and nonlinear transmission experiments, including a measurement at 1500 nm that established a real-valued $\gamma_{\rm rot} = (8 \pm 2) \times 10^{-48}$ m^5 V^{-2}, a measurement at 1180 nm that gave $\gamma_{\rm rot} = [(-25 \pm 10) + (37i \pm 5)] \times 10^{-48}$ m^5 V^{-2}, and a measurement at 960 nm that resulted in $\gamma_{\rm rot} = [(-10 \pm 6) + (7i \pm 7)] \times 10^{-48}$ m^5 V^{-2}.

have also confirmed that the amplitude of the laser-induced ultrasound does indeed grow as the square of the pulse energy [29], as expected for two-photon absorption.

Finally, in Fig. 7 we also add data points that have been determined through multiple individual measurements at 960, 1180, and 1500 nm. We note that for the DFWM measurement below ∼1050 nm, the linear absorption from this molecule starts to become significant, while the nonlinear two-photon absorption is not as important anymore. In this shorter wavelength range, we used Eq. (20) to model the DFWM data, as described above. Figure 7 shows that the third-order polarizability data obtained at various wavelengths and with various methods are consistent with the same underlying spectrum.

We conclude this section with a note about the relationship between linear absorption and two-photon absorption. All our results for the wavelength dependence of the imaginary part of $\gamma_{\rm rot}$ are compatible with the statement that the two-photon absorption spectrum taken at frequency ω is proportional to the linear absorption spectrum taken at frequency 2ω in noncentrosymmetric molecules. This is to be expected for an isolated lowest excited state that can be reached both by one-photon and by two-photon transitions. Because of this, for the noncentrosymmetric molecules we have investigated it is possible to use the known linear absorption spectrum at a wavelength $\lambda/2$ to aid in the extraction of the imaginary part of $\gamma_{\rm rot}$ from the DFWM data at a wavelength λ. In other words, one can use the known wavelength dependence of the absorption near $\lambda/2$ as a constraint for the wavelength dependence of the absolute value of the imaginary part of $\gamma_{\rm rot}$ near λ. And this in turn aids in the determination of more precise values for the real part of $\gamma_{\rm rot}$, leading to a numerically stable and robust result, with a physically satisfactory transition from larger complex values to purely real values of $\gamma_{\rm rot}$. This procedure is especially useful in the regions where the real part of $\gamma_{\rm rot}$ goes through a zero crossing, and the imaginary part is small (for example, this occurs between 1300 and 1400 nm for molecule 1; see Fig. 7). In such wavelength regions, the concentration dependence of $\chi^{(3)}_{1111}(C)$ in DFWM is fairly flat and featureless, which would otherwise lead to a large uncertainty in the determination of $\gamma_{\rm rot}$.

VII. RESULTS

We applied the methods described in the previous sections to determine the dispersion of the complex third-order polarizability of the molecules presented in Fig. 1. The result for molecule 1 (TDMEE) has been shown in Fig. 7. The results for molecules 2 (DDMEBT) and 3 are shown in Figs. 8 and 9, respectively.

In general, the spectra that we obtained follow the broad qualitative description that is predicted by a single oscillator response. Equation (9) alone, which does not take into account vibrational broadening and neglects the contribution from higher excited states, is too crude an approximation to be used for accurate modeling of the observed dispersion, but it can be useful to identify the broad features of the expected behavior of the third-order polarizability near the two-photon resonance: the imaginary part of $\gamma_{\rm rot}$ peaking in correspondence with

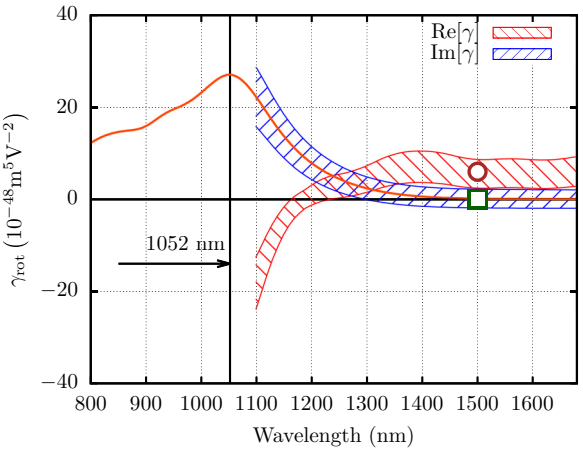

FIG. 8. (Color online) Spectrum of the third-order polarizability of molecule 2. Measurements at 1500 nm (given by round and square data points for real and imaginary part, respectively) established a value of $\gamma_{\rm rot} = (6 \pm 2) \times 10^{-48}$ m^5 V^{-2}. The peak of the two-photon resonance is expected to occur at $\lambda = 1052$ nm.

resonant two-photon absorption, with the real part starting with a finite positive value near zero frequency, increasing when approaching the resonance, and then transitioning to negative in coincidence with the two-photon resonance. For all three molecules discussed in this work, the resonant behavior of the imaginary part of $\gamma_{\rm rot}$ is the expected one. However, the maximum in the positive real part on the low-frequency part of the resonance is very shallow or nonexistent in our molecules, while the real part transitions to negative already at wavelengths longer than the center wavelength of the two-photon resonance and achieves a very large negative minimum at a wavelength only slightly shorter than the peak of the two-photon resonance. The molecule that shows the highest (positive) resonance enhancement of the real part of $\gamma_{\rm rot}$ is molecule 3, where the measured value of $\gamma_{\rm rot} = 9 \times 10^{-48}$ m^5 V^{-2} at 1500 nm is distinguishably larger than the off-resonant value observed at longer wavelengths. The

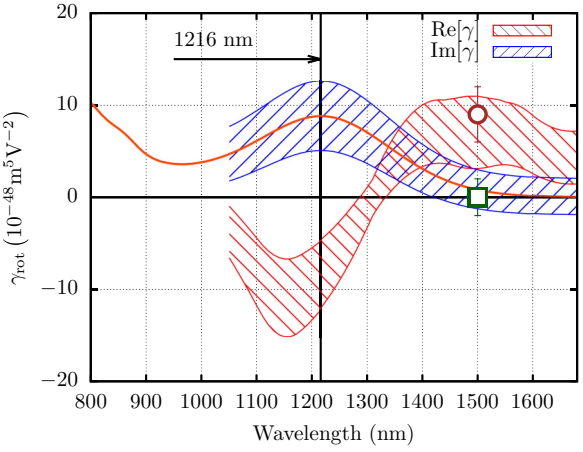

FIG. 9. (Color online) Spectrum of the third-order polarizability of molecule 3. A previous measurement of $\gamma_{\rm rot} = (9 \pm 2) \times 10^{-48}$ m^5 V^{-2} at 1500 nm (given by round and square data points for real and imaginary part, respectively) is included for comparison.

TABLE I. Properties and figures of merit for the molecules in Fig. 1. The five sections of the table give the parameters of each molecule, the derived fundamental limits, the experimental third-order polarizability at a wavelength of 1.5 μm, the experimental peak imaginary part of the third-order polarizability on the two-photon resonance, and the experimental ratio between imaginary part on resonance and real part off-resonance, as defined in Eq. (12). The first section lists the molar mass M in units of g/mol, the number of π electrons N_π, the position of the longest wavelength optical transition $\lambda_{\rm max}$ in nm, the extinction coefficient at $\lambda_{\rm max}$ in units of cm^{-1} M^{-1}, and the optical transition energies E_{10} and E_{20} (estimated) in eV. All third-order polarizabilities are in units of 10^{-48} m^5 V^{-2}. The experimental values are accompanied by the figures of merits we derive from them: the specific $\tilde{\gamma}_{\rm rot}$ in units of 10^{-23} m^5 kg^{-1} V^{-2}, and the intrinsic $\gamma_{\rm I}$ (dimensionless), which are given both for the real-valued third-order polarizabilities at 1.5 μm and for the imaginary parts of the third-order polarizability on the peak of the two-photon resonance.

	1	2	3
M	246.27	416.47	448.24
N_π	16	26	26
$\lambda_{\rm max}$	591	526	608
$\epsilon(\lambda_{\rm max})$	36990	45262	35065
E_{10}	2.09	2.36	2.04
E_{20}	3.60	4.45	3.16
$\gamma_{\rm k}$	662	976	2014
${\rm Im}[\gamma_{\rm k}^{\rm res}]$	11082	17103	36182
$R = {\rm Im}[\gamma_{\rm k}^{\rm res}]/\gamma_{\rm k}$	16.6	17.5	17.8
$\gamma_{\rm rot}(1.5\ \mu{\rm m})$	8 ± 2	6 ± 2	9 ± 2
$\tilde{\gamma}$	1.96	0.87	1.21
$\gamma_{\rm I} = \gamma_{\rm rot}/\gamma_{\rm k}$	0.0121	0.0061	0.0045
${\rm Im}[\gamma_{\rm rot}^{\rm res}]$	35 ± 10	25 ± 10	10 ± 5
${\rm Im}[\tilde{\gamma}_{\rm rot}^{\rm res}]$	8.56	3.61	1.3435
$\gamma_{\rm I}^{\rm res} = \gamma_{\rm rot}^{\rm res}/\gamma_k^{\rm res}$	0.0032	0.0015	0.0003
$R_{ex} = {\rm Im}[\gamma_{\rm rot}^{\rm res}]/\gamma_{\rm rot}^{\omega\to 0}$	5	4	1.6

spectrum in Fig. 9 confirms this, showing at this wavelength an enhancement of the real part, together with a still negligible imaginary part.

The data on the wavelength dependence of the third-order polarizability that we have obtained also allow us to determine, for each investigated molecule, the peak two-photon absorption cross section as well as the long-wavelength region for which the real part of the third-order polarizability becomes wavelength independent, taking on its off-resonant value in the zero-frequency limit.

We list the main properties of each molecule in Table I, together with the figure of merits that can be derived from them (i.e., the specific and intrinsic values of the third-order polarizability in the zero-frequency limit and on the peak of the two-photon resonance) and some experimental values of the third-order polarizability. The fundamental limits to the off-resonant and resonant third-order polarizability, necessary to obtain the intrinsic third-order susceptibility values, are calculated from the linear absorption spectra and the number of conjugated electrons (estimated as twice the number of multiple bonds in the conjugated system). Table I also gives the first and second excited-state energies, E_{10} and E_{20}, that

we used to obtain the fundamental limits for two-photon absorption (together with $\Gamma_{10} = 0.25$ eV; see below). We note that the value of the third-order polarizability at 1.5 μm that is given in this table is off resonant for molecules 1 and 2, but is resonantly enhanced by almost a factor of 2 for molecule 3. It is interesting to see, from the last section of the table, that the strength of the peak imaginary part of $\gamma_{\rm rot}$ and of the off-resonant real value are correlated. This is most clearly visible for molecules 1 and 2, which are off-resonant at $\lambda = 1.5$ μm and are also closest to the fundamental limit. This observation validates the approach we used above to derive a fundamental limit for the imaginary part of the third-order polarizability. On the other hand, the longest-wavelength two-photon resonance of molecule 3 is significantly weaker than in the other molecules, even though it is in the same spectral region as molecule 1.

We refer to Refs. [10,11,13,15] for a discussion of the off-resonant responses of the molecules in Table I. In the following we examine their resonant third-order nonlinearities, compare their corresponding two-photon absorption values to the literature, and discuss how off-resonant and on-resonance third-order polarizabilities relate to both the fundamental limits and to the size of a molecule.

The two-photon absorption cross sections calculated from the peak value of the imaginary part of $\gamma_{\rm rot}$ using Eq. (7) and a refractive index of 1.42 are shown in Table II, together with the corresponding values for two molecules that have been specifically developed for two-photon absorption applications, AF-50 [33] and AF-450 [34]. We chose to compare to AF-50 because it is a molecule not much larger than those we investigated here, and because it is a compound widely cited in the literature dedicated to two-photon absorption. It is important to point out that the two-photon cross section values that we report here are those that exclude the effects of excited-state absorption, which is known to deliver overinflated two-photon absorption cross sections in nonlinear transmission experiments performed using nanosecond pulses [33]. Table II also gives the fundamental limits for two-photon absorption as we calculate them, using (14), for the molecules in Table I as well as for AF-50 and AF-450. The excited-state energies used for this calculation are $E_{10} = 3.2$ eV and $E_{20} = 4.0$ eV for AF-50, and $E_{10} = 2.98$ eV and $E_{20} = 3.14$ eV for AF-450. The constant Γ_{10} is related to the width of the absorption band corresponding to the first excited state, and its influence on the fundamental limit for resonant two-photon absorption as given by (14) is essentially that of decreasing the peak value proportionally to the width of the resonance. Inspection of the absorption spectra reveals that the width of the lowest energy absorption line is similar for all molecules that we have investigated, and also for AF-50 and AF-450 [33,34]. To simplify comparisons, we used a value $\Gamma_{10} = 0.25$ eV for all fundamental limit calculations presented here.

We first discuss molecule 3. The data show that this molecule is the least efficient in its third-order nonlinear optical properties among those we have investigated. However, this molecule does show a resonance enhancement of the positive third-order polarizability near $\lambda = 1.5$ μm, with a relatively high value for $\gamma_{\rm rot}$ that is essentially real valued. Because of this resonance enhancement, this molecule has a specific third-order polarizability at 1.5 μm that is 50% larger than molecule 2, which indicates that $\chi^{(3)}$ of a solid-state assembly of molecule 3 has the potential to exceed that of molecule 2, whose supramolecular assemblies have been successfully used for all-optical switching [12,17,18]. At the same time, at $\lambda = 1.5$ μm the imaginary part of $\gamma_{\rm rot}$ remains negligible for this molecule. Development of molecules with this kind of resonance enhancement could be interesting for applications near telecommunication wavelengths. But apart from this aspect, molecule 3 is relatively weak from all other points of view, hinting at a fundamental inefficiency in its design compared to molecules 1 and 2. As an example, molecule 3 has the same number of π electrons (N_π) as molecule 2, but a lower intrinsic $\gamma_{\rm I}$ (because the lower energy of its first optical transition implies a much larger $\gamma_{\rm k}$).

Another distinguishing feature of molecule 3 is that it is the one with two clear optical transitions close to each other in energy, and the higher energy transition is stronger than the lower energy transition. The fact that this molecule has two competing charge-transfer transitions from either of the two dimethylamino donor groups to the cyano acceptors [15] may be a factor that leads to its inefficiency. While molecule 2 also has two almost independent conjugated subsystems caused by its nonplanar structure, the system that contains the triple bond clearly dominates its linear and nonlinear properties. For molecule 3, on the other hand, the two conjugated subsystems seem to compete with each other. This picture is also supported by comparing with molecule 1, which has the best figures of merit overall and the record for the highest efficiency, and consists of just one conjugated system.

TABLE II. Comparison of the fundamental limits for two-photon absorption cross sections, experimental values, and two-photon absorption figure of merits for the molecules studied in this work (Fig. 1) and for two two-photon-absorbing compounds from the literature, AF-50 [33] and AF-450 [34]. Apart from the experimental cross-section values for the molecule called AF-50 and the molecule called AF-450, which were taken from the literature [33,34], the theoretical and experimental values of all two-photon absorption cross sections have been calculated assuming a refractive index of 1.42. The last two columns give the specific and the intrinsic two-photon absorption cross sections.

	N_π	M (g/mol)	λ_{TPA} (nm)	Im$[\gamma_k^{\rm res}]$ (10^{-45} m^5 V^{-2})	σ_k^p (10^3 GM)	σ (10^{-20} cm^4/GW)	σ^p (GM)	$\tilde{\sigma}^p$ (10^{25} GM/kg)	σ_I^p [10^{-3}]
1	16	246.27	1182	11.1	89.0	1.70	284	69.5	3.19
2	26	416.47	1054	17.0	173	1.36	256	37.1	1.48
3	26	448.24	1216	35.8	272	0.47	76	10.3	0.28
AF-50	32	707.09	796	11.4	213	0.12	30	2.6	0.14
AF-450	90	1916.9	779	156	2537	0.87	222	7.0	0.08

Molecule 2 has a value of $\gamma_{\rm rot}$ that is approximately 75% that of molecule 1, both on and of resonance. The difference between molecule 1 and 2 is mainly related to their relative sizes: The additional group added to molecule 2 adds mass and size to the molecule, decreasing $\tilde{\gamma}$. Moreover, since we count all the electrons in the two conjugated subsystems of molecule 2 despite the fact that the conjugation is broken by the nonplanar structure, we obtain a larger value for the quantum limits, leading to a decrease in γ_I and $\gamma_I^{\rm res}$. In other words, the figures of merit of molecule 2 are worse than for molecule 1 because of the additional group that gives molecule 2 a nonplanar structure but does not significantly add to its nonlinearity, which is basically determined by a subsystem that is very similar to molecule 1. But at the same time the nonplanar structure of molecule 2 is the key to its ability to form high optical quality solid-state assemblies with a large $\chi^{(3)}$ [12,13], which is the very important practical property that allowed it to be successfully used for all-optical switching applications [17–19].

The fact that molecule 1 has the highest $\gamma_{\rm I}$ and $\gamma_{\rm I}^{\rm res}$ indicates that this molecule is the most efficient of the three, both in respect to its off-resonant response, and in respect to its two-photon absorption. Molecule 1 has a compact, fully conjugated design and is the smallest of the molecules considered here, which ultimately means that this molecule is able to use all the π electrons in its extended conjugated system in an optimum way, as is also shown by the fact that it has a low value of its first excited-state energy despite its small size [11]. Unfortunately, molecule 1 cannot produce high-quality dense assemblies like molecule 2 [12].

From the point of view of pure two-photon absorption efficiency, TDMEE and DDMEBT (molecules 1 and 2) have both the largest specific and the largest intrinsic two-photon absorption cross sections (see the last two columns of Table II).

But the most striking observation is how much larger the two-photon absorption properties of these molecules are in comparison to AF-50, a molecule specifically developed for two-photon absorption that is representative of a large class of compounds [33,35,36] and that has been often used as a benchmark molecule. In particular, molecule 1 (TDMEE) has a small conjugated system that is about half the size of AF-50, but it has an almost ten times larger two-photon absorption cross section, comparable with AF-450 [34], an even larger molecule. In fact, the two-photon cross sections of molecules 1 and 2 are comparable, within a factor of $\sim$4, to the optimal two-photon absorbers discussed in Ref. [37], even though molecules 1 and 2 are significantly smaller molecules.

These facts are quantitatively very well described by the two last columns of Table II, which give the intrinsic and specific two-photon absorption cross sections obtained by dividing the experimentally observed values by the quantum limit given by Eq. (14) and by the molecular mass, respectively. Molecules 1 and 2 dominate the rest of the field by a significant amount. This reflects both the potential of obtaining large two-photon coefficients in the solid state (realized for molecule 2), and also the intrinsic efficiency with which these molecules can interact with electromagnetic waves in a two-photon process.

The important conclusion that one can draw from all these observations is that the compounds presented in this work may represent a new category of two-photon absorbers that is worth investigating. The noncentrosymmetric substitution with strong donor and acceptor groups around a compact conjugated core is the key factor that distinguishes the molecules of Fig. 1 from other approaches like those described in Ref. [37]. The fact that in these compounds donor-acceptor substitution effectively results in the control and reduction of the energy of the first optical transition [11] may also play an important role in increasing their two-photon absorption efficiency.

Further, the ability to obtain large two-photon absorption cross sections in smaller molecules also has important practical consequences. The example that clearly illustrates this fact is molecule 2 (DDMEBT), which has been found to condense from the vapor phase into a dense single-component supramolecular assembly that is of high optical quality and has essentially the characteristics of an optical glass [12]. The large specific two-photon absorption cross section of this molecule directly implies an exceptionally large two-photon absorption coefficient in the solid-state material obtained in this way. As a practical rule of thumb, multiplying the specific two-photon absorption cross sections given in Table II, in units of 10^{25} GM/kg, by 0.6242 gives the bulk two-photon absorption coefficient β in units of cm/GW for a material with the density of water and a photon energy of 1 eV (wavelength of 1.24 μm). We estimate the bulk two-photon absorption coefficient of a DDMEBT molecular assembly [13] to be of the order of 10–20 cm/GW near 1050 nm, a very large value which can be compared to the value of 26 cm/GW observed in GaAs at 1064 nm [38], where it is determined by interband excitation. By following the design principles embodied in the DDMEBT molecule, it should therefore become possible to develop custom-designed two-photon absorbers as powerful as interband transitions in GaAs, but in an organic material where the spectral position of the two-photon resonance can be designed and tuned thanks to the flexibility of organic chemistry.

VIII. CONCLUSION

We demonstrated a flexible, robust method to automatically obtain the full dispersion of the real and imaginary parts of the third-order polarizability of molecules in solution. Using this method, we determined the third-order nonlinear dispersion in three molecules that have been investigated previously only at a wavelength of 1.5 μm. The spectroscopic data that we obtained by the automatic method is consistent with several other experiments we performed, namely DFWM, Z scan, nonlinear transmission, and laser-induced ultrasound.

In the three compounds we studied, we determined the peak two-photon absorption cross section, and wavelength regions with enhanced real-valued third-order polarizability between the zero-frequency limit and the first two-photon resonance. We also derived an expression for the fundamental limit to the two-photon absorption cross section for the lowest energy two-photon transition in noncentrosymmetric molecules, and we used it to show that the compounds we investigated have an extraordinary efficiency for two-photon absorption when compared to other benchmark molecules such as AF-50,

matching similar results obtained earlier for off-resonant nonlinearities in the same molecules.

These findings highlight the importance of designs based on donor-acceptor substitution in small organic molecules—a principle previously demonstrated for off-resonant nonlinearities—for the development of two-photon-absorbing and optical limiting materials. This is particularly important given the fact that small donor-acceptor–substituted molecules such as molecule 2 do not only have exceptional nonlinear optical and two-photon absorption properties, but they can also be combined in dense supramolecular assemblies with a high optical quality that can be incorporated in existing integrated optics technologies [17–19].

ACKNOWLEDGMENT

This material is based upon work supported by the National Science Foundation under Grant No. DMR-1408862.

[1] R. W. Hellwarth, Prog. Quantum Electron. **5**, 1 (1977).
[2] P. N. Butcher and D. Cotter, *The Elements of Nonlinear Optics* (Cambridge University Press, Cambridge, England, 1991).
[3] P. E. Powers, *Fundamentals of Nonlinear Optics* (CRC, Boca Raton, 2011).
[4] S. S. Andrews, J. Chem. Ed. **81**, 877 (2004).
[5] M. Göppert-Mayer, Ann. Phys. **401**, 273 (1931).
[6] M. G. Kuzyk, Phys. Rev. Lett. **85**, 1218 (2000).
[7] M. G. Kuzyk, Opt. Lett. **25**, 1183 (2000).
[8] M. G. Kuzyk, Phys. Rev. Lett. **90**, 039902(E) (2003).
[9] J. Zhou and M. G. Kuzyk, J. Phys. Chem. C **112**, 7978 (2008).
[10] J. C. May, J. H. Lim, I. Biaggio, N. N. Moonen, T. Michinobu, and F. Diederich, Opt. Lett. **30**, 3057 (2005).
[11] J. C. May, I. Biaggio, F. Bures, and F. Diederich, Appl. Phys. Lett. **90**, 509 (2007).
[12] B. Esembeson, M. Scimeca, T. Michinobu, and F. Diederich, Adv. Mater. **20**, 4584 (2008).
[13] M. T. Beels, M. S. Fleischman, I. Biaggio, B. Breiten, M. Jordan, and F. Diederich, Opt. Mater. Express **2**, 294 (2012).
[14] I. Biaggio, in *Handbook of Organic Materials for Optical and (Opto)electronic Devices: Properties and Applications*, edited by O. Ostroverkhova (Woodhead, Cambridge, 2013), Chap. 5, pp. 170–189.
[15] M. Chiu, B. Jaun, M. T. Beels, I. Biaggio, J.-P. Gisselbrecht, C. Boudon, W. B. Schweizer, M. Kivala, and F. Diederich, Org. Lett. **14**, 54 (2012).
[16] T. Michinobu, J. C. May, J. H. Lim, C. Boudon, J.-P. Gisselbrecht, P. Seiler, M. Gross, I. Biaggio, and F. Diederich, Chem. Commun., 737 (2005).
[17] C. Koos, P. Vorreau, T. Vallaitis, P. Dumon, W. Bogaerts, R. Baets, B. Esembeson, I. Biaggio, T. Michinobu, F. Diederich, W. Freude, and J. Leuthold, Nat. Photon. **3**, 216 (2009).
[18] T. Vallaitis, S. Bogatscher, L. Alloatti, P. Dumon, R. Baets, M. L. Scimeca, I. Biaggio, F. Diederich, C. Koos, W. Freude, and J. Leuthold, Opt. Express **17**, 17357 (2009).
[19] J. Leuthold, W. Freude, J. Brosi, R. Baets, P. Dumon, I. Biaggio, M. Scimeca, F. Diederich, B. Frank, and C. Koos, Proc. IEEE **97**, 1304 (2009).
[20] M. G. Kuzyk, J. Chem. Phys. **119**, 8327 (2003).
[21] K. Tripathy, J. P. Moreno, M. G. Kuzyk, B. J. Coe, K. Clays, and A. M. Kelley, J. Chem. Phys. **121**, 7932 (2004).
[22] J. Armstrong, N. Bloembergen, J. Ducuing, and P. Pershan, Phys. Rev. **127**, 1918 (1962).
[23] M. Rumi and J. W. Perry, Adv. Opt. Photon. **2**, 451 (2010).
[24] M. Sheik-Bahae, A. A. Said, T.-H. Wei, D. J. Hagan, and E. W. Van Stryland, IEEE J. Quantum Electron. **26**, 760 (1990).
[25] U. Gubler and C. Bosshard, Phys. Rev. B **61**, 10702 (2000).
[26] D. Milam, Appl. Opt. **37**, 546 (1998).
[27] S. Santran, L. Canioni, L. Sarger, T. Cardinal, and E. Fargin, J. Opt. Soc. Am. B **21**, 2180 (2004).
[28] F. P. Strohkendl, L. R. Dalton, R. W. Hellwarth, H. W. Sarkas, and Z. H. Kafafi, J. Opt. Soc. Am. B **14**, 92 (1997).
[29] J. C. May, Ph.D. Dissertation, Lehigh University, 2007.
[30] R. Miller, R. Casalegno, K. A. Nelson, and M. Fayer, Chem. Phys. **72**, 371 (1982).
[31] K. A. Nelson, R. D. Miller, D. Lutz, and M. Fayer, J. Appl. Phys. **53**, 1144 (1982).
[32] K. A. Nelson, R. Casalegno, R. D. Miller, and M. Fayer, J. Chem. Phys. **77**, 1144 (1982).
[33] O.-K. Kim, K.-S. Lee, H. Y. Woo, K.-S. Kim, G. S. He, J. Swiatkiewicz, and P. N. Prasad, Chem. Mater. **12**, 284 (2000).
[34] R. Kannan, G. S. He, T.-C. Lin, P. N. Prasad, R. A. Vaia, and L.-S. Tan, Chem. Mater. **16**, 185 (2004).
[35] G. S. He, L. Yuan, N. Cheng, J. D. Bhawalkar, P. N. Prasad, L. L. Brott, S. J. Clarson, and B. A. Reinhardt, J. Opt. Soc. Am. B **14**, 1079 (1997).
[36] J. W. Baur, M. D. Alexander, M. Banach, L. R. Denny, B. A. Reinhardt, R. A. Vaia, P. A. Fleitz, and S. M. Kirkpatrick, Chem. Mater. **11**, 2899 (1999).
[37] M. Albota, D. Beljonne, J.-L. Brédas, J. E. Ehrlich, J.-Y. Fu, A. A. Heikal, S. E. Hess, T. Kogej, M. D. Levin, S. R. Marder *et al.*, Science **281**, 1653 (1998).
[38] A. A. Said, M. Sheik-Bahae, D. J. Hagan, T. H. Wei, J. Wang, J. Young, and E. W. V. Stryland, J. Opt. Soc. Am. B **9**, 405 (1992).